Received: 10 October 2023 | Accepted: 23 February 2024

DOI: 10.1111/1462-2920.16605

BRIEF REPORT

ENVIRONMENTAL MICROBIOLOGY

A single *Prochlorococcus* ecotype dominates the tropical Bay of Bengal with ultradian growth

Jonathan Grone[1] | **Camille Poirier**[1] | **Kathleen Abbott**[2,3] | **Fabian Wittmers**[1,4] | **Gualtiero Spiro Jaeger**[3] | **Amala Mahadevan**[3] | **Alexandra Z. Worden**[1,4]

[1]Ocean EcoSystems Biology Unit, GEOMAR Helmholtz Centre for Ocean Research Kiel, Kiel, Germany

[2]Massachusetts Institute of Technology, Cambridge, Massachusetts, USA

[3]Woods Hole Oceanographic Institution, Woods Hole, Massachusetts, USA

[4]Marine Biological Laboratory, Woods Hole, Massachusetts, USA

Correspondence
Alexandra Z. Worden, Marine Biological Laboratory, Woods Hole, MA, USA.
Email: azworden@mbl.edu

Funding information
Gordon and Betty Moore Foundation, Grant/Award Number: 3788; Simons Foundation (BIOS-SCOPE); Office of Naval Research, Grant/Award Number: N000014-17-1-2390; National Science Foundation, Grant/Award Number: 2230811

Abstract

The Bay of Bengal (BoB) spans >2.2 million km^2 in the northeastern Indian Ocean and is bordered by dense populations that depend upon its resources. Over recent decades, a shift from larger phytoplankton to picoplankton has been reported, yet the abundance, activity, and composition of primary producer communities are not well-characterized. We analysed the BoB regions during the summer monsoon. *Prochlorococcus* ranged up to 3.14×10^5 cells mL^{-1} in the surface mixed layer, averaging $1.74 \pm 0.46 \times 10^5$ in the upper 10 m and consistently higher than *Synechococcus* and eukaryotic phytoplankton. V1-V2 rRNA gene amplicon analyses showed the High Light II (HLII) ecotype formed 98 ± 1% of *Prochlorococcus* amplicons in surface waters, comprising six oligotypes, with the dominant oligotype accounting for 65 ± 4% of HLII. Diel sampling of a coherent water mass demonstrated evening onset of cell division and rapid *Prochlorococcus* growth between 1.5 and 3.1 div day^{-1}, based on cell cycle analysis, as confirmed by abundance-based estimates of 2.1 div day^{-1}. Accumulation of *Prochlorococcus* produced by ultradian growth was restricted by high loss rates. Alongside prior Arabian Sea and tropical Atlantic rates, our results indicate *Prochlorococcus* growth rates should be reevaluated with greater attention to latitudinal zones and influences on contributions to global primary production.

INTRODUCTION

The Bay of Bengal (BoB) provides important ecosystem services to hundreds of millions of people in its densely populated coastal areas. Characteristic features of the BoB that set it apart from many other ocean regions include a north–south salinity gradient (lower salinity in the north due to riverine discharge) and salinity-driven stratification due to fresher waters at the surface (Mahadevan et al., 2016). Like subtropical gyres and other tropical ecosystems, the BoB has an abundance of picophytoplankton (Larkin et al., 2020; Strauss et al., 2023) and it has been proposed that picocyanobacteria are increasing in abundance while larger phytoplankton are decreasing based on remote sensing observations (Löscher, 2021). Such shifts have important implications for primary production and marine food webs.

Phytoplankton communities remain understudied in offshore regions of the BoB, and oceanographic contextual physicochemical information in general has been limited. Several BoB studies have focused on diatoms and large eukaryotic phytoplankton. Nevertheless, both *Prochlorococcus* (Biller et al., 2015) and *Synechococcus* have been reported in BoB waters (Angelova et al., 2019; Strauss et al., 2023), and survey

sampling of the upper 7 m shows that the *Prochlorococcus* High Light II (HLII) ecotype can have high relative amplicon abundances extending from the BoB into the Southern Indian Ocean (Larkin et al., 2020; Strauss et al., 2023). Here, we examine the abundance, diversity and growth of *Prochlorococcus* due to its reported importance and indications that it is increasing in importance in this complex ecosystem.

EXPERIMENTAL PROCEDURES

Sampling

The MISO-BoB-2018 cruise took place between 6 June and 22 June 2018, onboard the *R/V Thomas G. Thompson*. Biological sampling involved 27 CTD casts and additional flowthrough sampling in regional clusters, as in Figure 1A. CTD casts were performed at different times throughout the day and night, with an effort to cover the early morning (06:00–06:30) more consistently. Sampling depths were chosen according to physical and biological properties and always included the surface, the subsurface chlorophyll maximum (SCM) and the top of the oxygen minimum zone. The intake depth of the ship's flowthrough system used for the 36 h *Diel* sampling was 7 m, with collection every 2 h (19 samples in total). Flow cytometry samples were fixed with 25% electron microscopy grade glutaraldehyde (final concentration, 0.25%) for 20 min at room temperature in the dark, flash-frozen in liquid nitrogen, and stored at −80°C. For DNA, 0.5–1 L of water was filtered onto a 0.2-micron pore-size Supor filter and immediately frozen at −80°C. Temperature and salinity data were collected from the flowthrough system using an SBE 45 MicroTSG thermosalinograph (Sea-Bird Scientific) with a sampling frequency of 1 Hz. Note that absolute salinity and conservative temperature were calculated from observations using the Gibbs Seawater Toolbox (McDougall & Barker, 2011) and a Hampel filter, using a sliding window of 500 s to replace data outside of the range of 3 standard deviations with the running median.

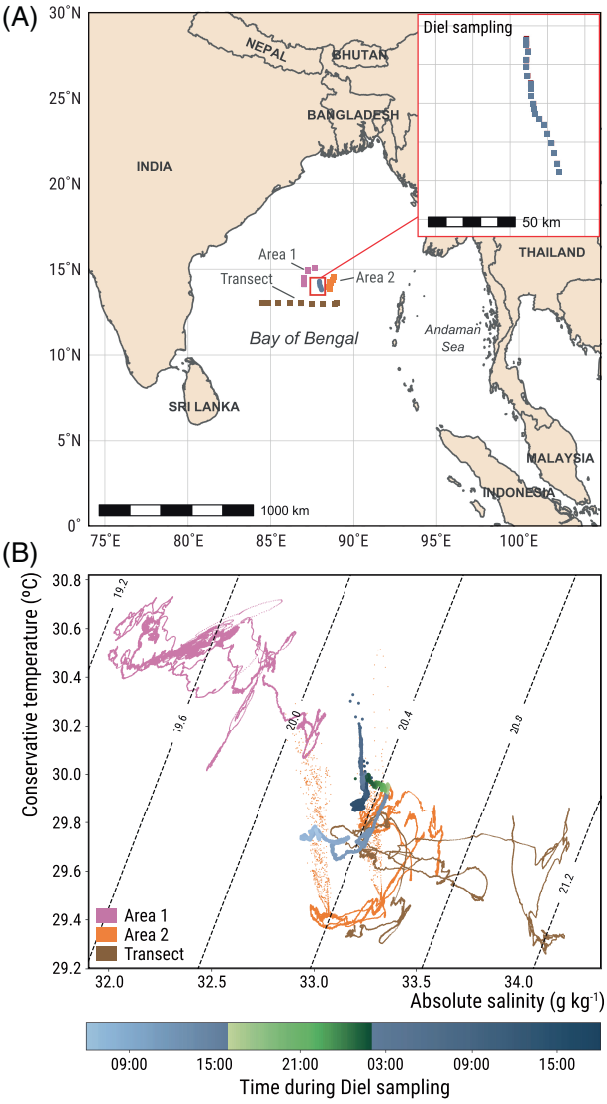

FIGURE 1 Water mass characteristics of sampled regions in the Bay of Bengal. (A) Sampling stations are indicated by squares and grouped by geographical arrangement and physical properties as *Area 1* (pink), *Area 2* (orange) and *Transect* (brown). Locations sampled using ship flowthrough (blue) and used for the *Diel* are expanded in the inset. (B) Surface temperature—salinity from the flowthrough system's thermosalinograph in the Areas as above and during the diel (blue and green colour gradients corresponding to the time of day). The green colour gradient highlights the first *Prochlorococcus* growth phase during the diel sampling.

Flow cytometry and cell cycle analyses

FCM samples were analysed using a BD Influx Cell Sorter equipped with a 488 nm 200 mW laser and a 457 nm 300 mW laser. Measured cell characteristics were forward angle light scatter (set as the trigger parameter), side scatter, red autofluorescence (692/40 nm band-pass filter, for chlorophyll *a*), orange autofluorescence (572/27 nm band-pass filter, for phycoerythrin) and green fluorescence (520/35 nm band-pass filter). Before each run, fluorescent polystyrene beads were added (0.75 μm yellow–green, Polysciences, Inc.). Samples were run for 8 min at a flow rate of ~23 μL min^{-1} measured with an inline flow meter (Sensirion), with the final volume run also determined by weighing.

For cell cycle analyses, a second run was performed after staining Diel samples with SYBR Green I (0.5X final concentration; Thermo Fisher Scientific Inc., Waltham, MA, USA) and incubating for 15 min. In this second run, samples were measured for 2 min at ~23 μL min^{-1} with SYBR Green fluorescence as the trigger, which was measured via a 520/35 nm band-pass filter. Population analysis was performed using FlowJo™ v10.8.1

(Becton Dickinson and Company, 2023), according to established methods (Sudek et al., 2015). To obtain the fractions of cells in the G_1, S and G_2 phases in the *Prochlorococcus* population at a given time point, the Watson cell cycle model implemented in FlowJo was used. Using a histogram of the flow cytometric measurements of SYBR Green fluorescence at 520/35 nm as a proxy for DNA content, the model assumes two Gaussian populations for the G_1 and G_2 phases and the S-phase population between those two. For each time point, the model parameters were adjusted to minimise the RMSD statistic. The denomination of the cell cycle phases as G_1, S and G_2 is originally intended only for the eukaryotic cell cycle and is used here as an analogue for the bacterial cell cycle of *Prochlorococcus* as commonly applied, for example by Shalapyonok et al. (1998).

To estimate biomass contributions from different phytoplankton groups the following conversion factors were used: 39 fg C cell^{-1} for *Prochlorococcus* (green), 82 fg C cell^{-1} for *Synechococcus* (orange), 530 fg C cell^{-1} for picoeukaryotic phytoplankton as lower bound estimate (light blue), all from Worden et al. (2004), and 730 fg C cell^{-1} for picoeukaryotic phytoplankton as upper bound estimate (dark blue) (Grob et al., 2007).

DNA extractions and amplicon sequencing

Genomic DNA was extracted using a modified Qiagen DNeasy™ plant kit (Qiagen) with preceding freeze–thaw and bead-beating steps for thermal and mechanical cell lysis as described by Demir-Hilton et al. (2011). Eluted DNA extracts were stored at −80°C. The V1-V2 region of the 16S rRNA gene was amplified using primers and PCR steps as described by Hoadley et al. (2021), targeting bacteria and plastid-bearing eukaryotes. Sequencing of paired-end libraries was performed using the Illumina MiSeq platform. Steps for extraction and sequencing were the same for the 7 Diel DNA samples, where 1 L of seawater from the ship's flow-through system was filtered.

16S rRNA gene amplicon analyses

Demultiplexed V1-V2 16S rRNA amplicons were quality-controlled and trimmed with cutadapt (v2.6) using default settings (Martin, 2011). Amplicons were denoised, chimeric sequences removed and Amplicon Sequence Variants (ASVs) generated using dada2 (qiime2 plugin version 2020.11.1, settings–p-trunc-len-f 210–p-trunc-len-r 180) (Callahan et al., 2016). ASVs were taxonomically classified using best node placement in a Python 3 version of the phylogenetic placement pipeline PhyloAssigner (Vergin et al., 2013) and a series of consecutive 16S rRNA gene reference trees. The rewritten pipeline, as well as reference alignments and trees used, are available as open source via GitHub (https://github.com/BIOS-SCOPE/PhyloAssigner_python_UCSB). ASVs were first placed on a global 16S rRNA gene reference tree, as published by Vergin et al. (2013). Sequences placed on the cyanobacteria and plastid branches were extracted and analysed at higher resolution using a cyanobacteria and plastid reference tree (Sudek et al., 2015). Sequences classified as cyanobacteria were then further classified using a *Prochlorococcus* and *Synechococcus* tree, and the final *Prochlorococcus* taxonomy was generated from a refined *Prochlorococcus* 16S rRNA reference tree (Strauss et al., 2023).

Statistics and visualisation

All statistical calculations regarding biological data were performed in R (R Core Team, 2023) using Rstudio (Rstudio Team, 2022). Oligotyping was performed according to Eren et al. (2013). Statistics regarding physical data were performed as described in the Sampling section using Python (v3.7.9) (van Rossum & Drake, 1995). For the Kruskal–Wallis test (Figure S4), the R package psych (v2.3.6) was used after checking that the data met the test assumptions.

Temperature–salinity variability was visualised with a T–S plot (Figure 1B) using Python (v3.7.9) (van Rossum & Drake, 1995) with the packages numpy (v1.21.6), pandas (v1.2.0), matplotlib (v3.3.3) and gsw (v3.4.0). Other figures were generated in R (v4.1.1) (R Core Team, 2023) using RStudio (v1.4.1717) (RStudio Team, 2022) and the packages ggplot2 (v3.3.6), hrbrthemes (v0.8.0), phyloseq (v1.36.0), rnaturalearth (v0.1.0), rnaturalearthhires (v0.2.0), ggspatial (v1.1.5) and sf (v1.0-7).

RESULTS AND DISCUSSION

We performed an expedition through different regions of the BoB during the onset of the summer monsoon period in June 2018 (Spiro Jaeger et al., 2020). Sampling clusters were designed to determine spatial variation, with intensive sampling in two geographic areas: Areas 1 and 2 (Figure 1A). Another cluster, Diel, was within a coherent water mass between Areas 1 and 2, and high temporal resolution (through day and night) sampling was performed for subsequent cell cycle analysis. We also sampled broadly from east to west (Transect), south of the other clusters. Area 1, located in the northeast, had the warmest and freshest water in the surface layer (30.4 ± 0.1°C, 32.54 ± 0.29 g kg^{-1}), and the transect located in the south had the coldest and saltiest waters (29.5 ± 0.2°C, 33.53 ± 0.35 g kg^{-1}; Figure 1B). Thus, our sample set displayed rather

modest temperature and salinity gradients compared to the overall span of the BoB (Strauss et al., 2023). Flow cytometry samples were collected and analysed from 5 to 7 depths, typically 2–10 m (surface), the subsurface chlorophyll maximum (SCM; 50–85 m), and intermediate depths (Figure S1; Datasheet SA).

Prochlorococcus was the numerically dominant phytoplankton group in the surface for all regions studied (Figure 2A). The maximum surface *Prochlorococcus* concentration observed was 2.69×10^5 cells mL^{-1} (surface average $1.74 \pm 0.46 \times 10^5$ cells mL^{-1}, $n = 46$), and the overall maximum was 3.14×10^5 cells mL^{-1} (50 m), both occurring in the transect region, where *Synechococcus* was approximately an order of magnitude lower (surface average $2.11 \pm 1.21 \times 10^4$ cells mL^{-1}, $n = 46$) (Datasheet SA). In contrast, in the southwest summer monsoon during August/September of 2015, *Synechococcus* abundances (surface average $8.20 \pm 2.32 \times 10^4$ cells mL^{-1}, $n = 29$) were closer to *Prochlorococcus* (surface average $1.17 \pm 0.44 \times 10^5$ cells mL^{-1}, $n = 29$; Datasheet SB) (Strauss et al., 2023). These differences appear to be linked to the warmer temperatures in 2018 being unfavourable to *Synechococcus*, although other factors are likely important as well (Figure S2; Supporting Information Section S1). In addition, our study focused on more central and southward locations than those in the 2015 study, which extended further northwards. With respect to photosynthetic picoeukaryotes, surface concentrations in our study averaged $1.36 \pm 0.33 \times 10^3$ cells mL^{-1} ($n = 46$), with a maximum abundance of 2.68×10^4 cells mL^{-1} (60 m). *Prochlorococcus* also generally dominated at the SCM ($8.76 \pm 3.68 \times 10^4$ cells mL^{-1}, $n = 27$), followed by picoeukaryotes ($7.96 \pm 4.80 \times 10^3$ cells mL^{-1}, $n = 27$), and *Synechococcus* ($6.20 \pm 7.76 \times 10^2$ cells mL^{-1}, $n = 27$).

While *Prochlorococcus* abundances herein were in the same order of magnitude as observed in the 2015 BoB southwest summer monsoon (Strauss et al., 2023) and eastern Indian Ocean (Landry et al., 2022), they were higher than reported in other BoB studies (Gu

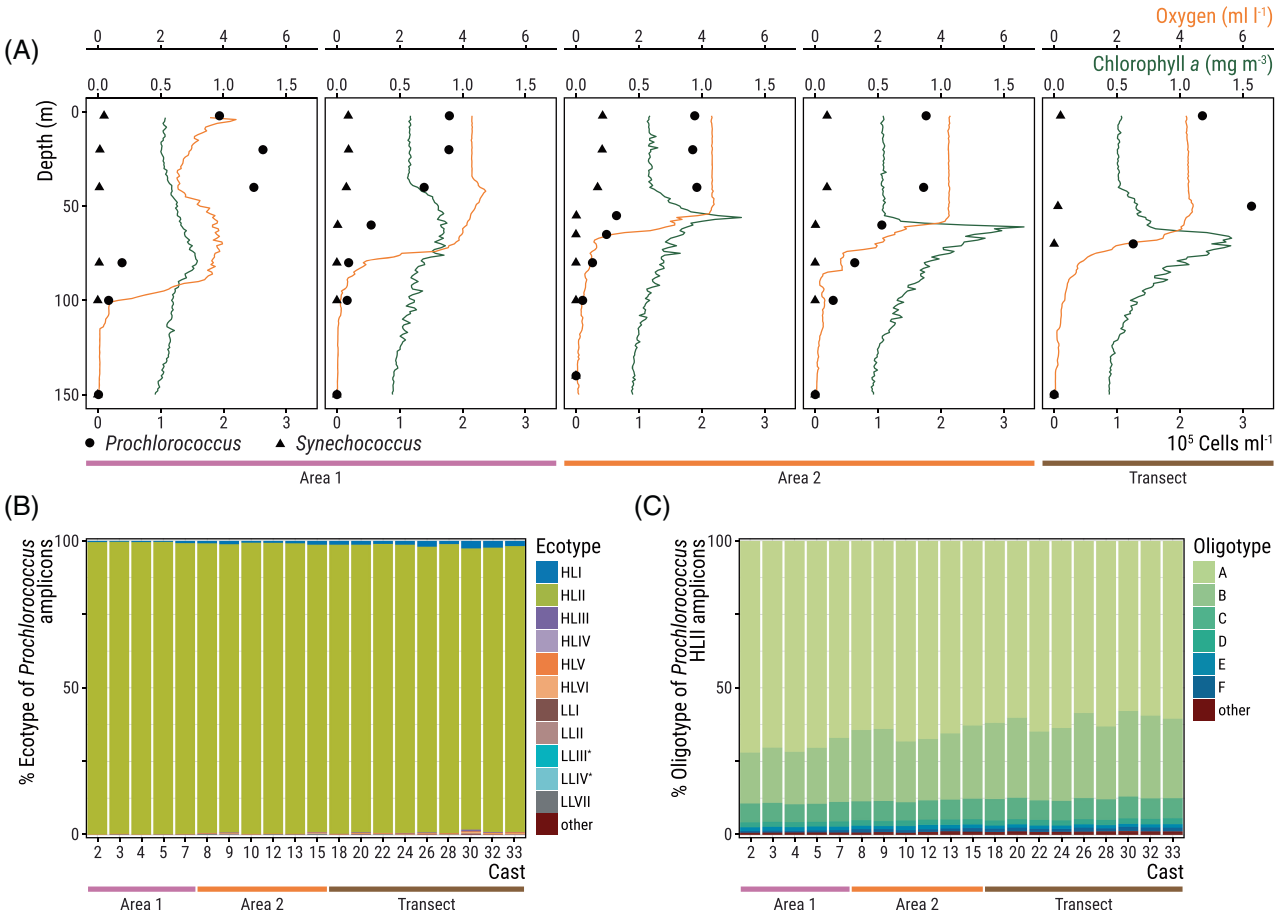

FIGURE 2 *Prochlorococcus* cells are highly abundant, leading to phytoplankton community dominance by the HLII Ecotype. (A) Flow cytometric profiles of *Prochlorococcus* (circles) and *Synechococcus* (triangles) show extreme dominance of the former. Also shown are O_2 concentrations [ml L^{-1}] (orange) and chlorophyll *a* concentrations derived from in vivo fluorescence [mg m^{-3}] (green) for five representative CTD casts, each performed at ~06:30 AM local time. Note that photosynthetic eukaryotes were also enumerated and averaged $1.39 \pm 0.32 \times 10^3$ cells mL^{-1} at the surface and $7.96 \pm 4.80 \times 10^3$ cells mL^{-1} at the SCM. (B) Relative abundances of *Prochlorococcus* ecotypes out of all *Prochlorococcus* amplicons, with groupings as in Figure 1A. Asterisks indicate ecotypes that were not detected in surface samples. (C) Relative abundances of oligotypes identified within the 119 *Prochlorococcus* HLII ASVs present in surface samples (~1–10 m).

et al., 2022; Mitbavkar et al., 2020; Wei et al., 2020). With respect to carbon biomass, *Prochlorococcus* is estimated to comprise ~70% of the phytoplankton biomass in BoB surface waters (Figure S1; see Supplementary Information). A clear SCM was observed in Area 2 and Transect, while *Prochlorococcus* cell abundances were relatively stable across the shallow mixed layer and declined rapidly below it (Figure S1), as in 2015 (Strauss et al., 2023). Unlike many tropical and subtropical water columns that are thermally stratified and where nutrients go below detection limits in the surface waters, here nutrients such as phosphate and nitrate were detectable at the surface (Datasheet SB).

To examine diversity, 16S rRNA gene V1-V2 amplicons were generated and analysed from surface samples using maximum likelihood methods and a reference 16S rRNA gene tree. Three hundred distinct *Prochlorococcus* V1-V2 16S rRNA Amplicon Sequence Variants (ASVs) were detected in CTD surface samples (Datasheet SC). Approximately one-third (119) were HLII, which contributed 98.2 ± 1.0% ($n = 20$) of all *Prochlorococcus* amplicons (Figure 2B; Datasheet SD). This pattern is consistent across sampling areas and previous BoB results (Larkin et al., 2020; Strauss et al., 2023). In addition, oligotypes were defined for *Prochlorococcus* ecotype HLII using the three single nucleotide polymorphisms with the highest entropy (Eren et al., 2013). HLII oligotype distributions were consistent across surface samples, with oligotypes A and B contributing 64.7 ± 4.3% and 23.6 ± 3.6% ($n = 20$) of HLII amplicons, respectively (Figure 2C). During the 36-h long Diel, the seven distributed time points where sequencing was performed showed consistent *Prochlorococcus* ecotype and HLII oligotype distributions throughout (Datasheet SE). Specifically, 98.7 ± 0.1% ($n = 7$) of *Prochlorococcus* amplicons were HLII, with 65.2 ± 0.9% and 23.2 ± 0.9% being oligotype A and B, respectively (Figure 3A,B), pointing to the coherence of the *Prochlorococcus* populations present. In the 2015 BoB study, HLII oligotype A was closer to 50% on the surface, with oligotype B being second to highest (Strauss et al., 2023). Based on different genetic markers, specifically rpoC1, alternating dominance of two HLII oligotypes was observed along a latitudinal transect across the BoB (Larkin et al., 2020). Moreover, based on the ITS marker, high relative

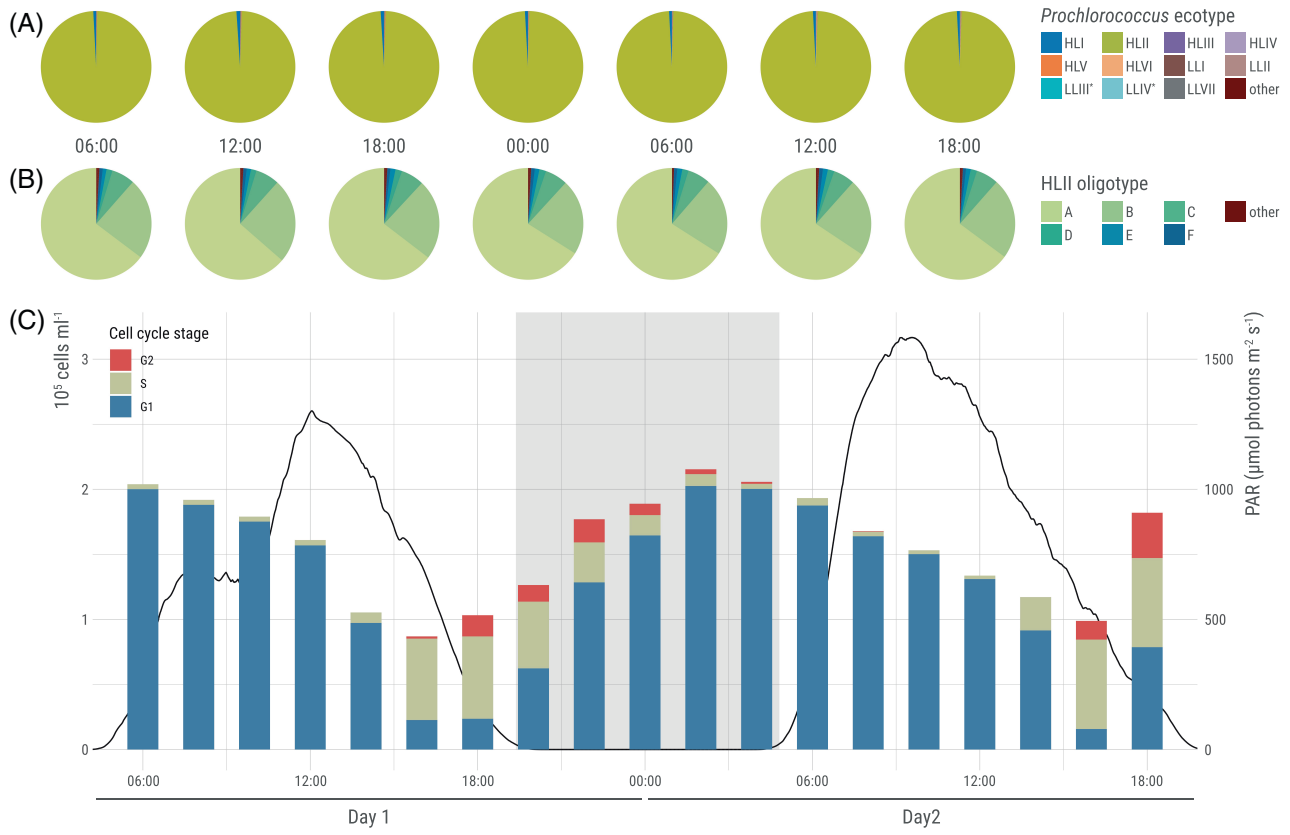

FIGURE 3 HLII *Prochlorococcus* expresses high and synchronised growth. (A) Relative fractions of different ecotypes present among *Prochlorococcus* ASVs for the time points with DNA sampling (every third sample, i.e., every 6 h, see Datasheet SE) during the diel sampling period. Asterisks indicate ecotypes that were not detectable in surface samples. (B) Relative fractions of the different oligotypes among all 119 *Prochlorococcus* HLII ASVs for the time points with DNA sampling (every third sample, i.e., every 6 h) during the diel sampling period. (C) Absolute cell counts of *Prochlorococcus* in G_1, S and G_2 cell cycle stages and rolling mean of the photosynthetically active radiation (PAR; black line) during the 36-h diel sampling period. The grey bar indicates nighttime.

abundances of a single oligotype within both *Prochlorococcus* and *Synechococcus* ecotypes have been reported in the subtropical Northeast Pacific (Ahlgren et al., 2019; Thompson et al., 2021). Thus, the dominance by a single oligotype (or haplotype), potentially in alternation with others, appears to be a common feature of the *Prochlorococcus* communities in tropical and subtropical environments.

Despite the coherence of the water mass sampled during the Diel, *Prochlorococcus* abundance changed markedly over the day–night period. Cell abundances were highest around 02:00 (local time) and thereafter incrementally decreased by >50% at ~16:00 h. *Prochlorococcus* increased from early evening into the night (Figure 3C). The use of the dsDNA stain SYBR Green and analysis by flow cytometry allowed us to observe chromosomal replication over the Diel (Shalapyonok et al., 1998). A first notable increase of S-phase cells was observed 2 h before the time of lowest cell abundances, by which point ~70% of cells were in S-phase. Moreover, two temporally offset peaks of G_2 cells were observed, indicating ultradian growth, that is, more than one round of division per day, as once observed in the Arabian Sea (Shalapyonok et al., 1998). The growth rate μ_{DNA} was calculated using

$$\mu_{DNA} = \frac{1}{n \times t_{S+G2}} \sum_{i=1}^{n} \ln[1 + f_{S+G2}(i)], \quad (1)$$

where n is the number of samples during a 24-h sampling period, t_{S+G2} is the combined duration of S and G_2 phases, and $f_{S+G2}(i)$ is the fraction of cells in S or G_2 in the sample i (Shalapyonok et al., 1998).

An important component of the above equation is t_{S+G2}, which can be determined by closely observing the periods of growth onset. In our data, a first notable increase in S-phase cell numbers can be seen on both days at 14:00 h, with a first net positive population growth 4 h later. On both days, the net population growth is more than double the number of S-phase cells at 14:00 h, suggesting that some of the newly divided cells went into S-phase after 14:00 h. The resulting duration of S and G_2 phases would thus be between 2 and 4 h. An alternative calculation of t_{S+G2} would be twice the time between (the first) peaks of the fractions in the S and G_2 phase, that is, 16:00 h and 18:00 h, respectively (Shalapyonok et al., 1998), resulting in a t_{S+G2} of 4 h. In both cases, temporal sampling resolution (every 2 h) causes a range of t_{S+G2} between 2 and 4 h. In the resulting calculation, maximum and minimum growth rates $\mu_{DNA_{max}}$ and $\mu_{DNA_{min}}$ were 2.12 and 1.06 day^{-1}, respectively, or 3.06 and 1.53 div day^{-1}, respectively. Estimating the growth rate by cell abundances with a model of dynamic mortality over the day (Figure 3A,B) results in a $\mu_{cell} = 1.47\ day^{-1}$, or 2.12 div day^{-1} (Figure S3). This rate falls within the range of rates based on cell cycle analysis (μ_{DNA}), supporting estimation of t_{S+G2} being between 2 and 4 h.

For comparison to the literature, we adopted the moderately conservative growth rate for the BoB (2.12 div day^{-1}), intermediate to the maximum and minimum calculations, and equal to the cell abundance-based rate. This is among the highest reported for *Prochlorococcus* in the Indian Ocean and elsewhere. Note that values reported as μ day^{-1} have been converted to div day^{-1} for comparison purposes. Other high rates in the Indian Ocean were observed in the Eastern Indian Ocean with ~1.44 div day^{-1} (Landry et al., 2022) and in the Arabian Sea at 1.42 div day^{-1} (Shalapyonok et al., 1998). Had we adopted the same methodology of an assumed stable mortality rate for a growth rate estimate based on cell abundances, as used in the latter study, our estimates of μ_{cell} would have increased to 3.53 div day^{-1} (see Supporting Information Section S2). The moderately conservative rate herein is akin to the maximum observed in the tropical Atlantic, 2.12 div day^{-1} (Agawin & Agustí, 2005), and exceeds the highest values we are aware of for the Pacific (0.92 div day^{-1}, Liu et al., 1999; ~0.95 div day^{-1}, Vaulot et al., 1995). Finally, one other study has reported varying, including higher rates, from a couple of locations in the Arabian Sea; however, this study used extremely different methodology (multiple size fractions of grazer exclusions, shipboard incubations, and flow cytometric cell counting of *Prochlorococcus* at much lower abundances) (Reckermann & Veldhuis, 1997). The extreme dominance of *Prochlorococcus* in the BoB is thus likely connected to its exceptionally rapid growth. Inferences from comparisons of metagenomic data suggest that the number of HLII replications per day peaks in the BoB relative to other parts of the Indian Ocean (Larkin et al., 2023). We recognise that water mass exchange could, in theory, have underpinned the large changes in cell abundance between time points. However, the spatial proximity of our sampling points, the small variations in conservative temperature (29.9 ± 0.1°C) and absolute salinity (33.24 ± 0.11 g kg^{-1}) during the Diel (Figure 1B), and the consistent genetic diversity profiles (Figure 3A,B) indicate minimal transport or exchange of water/populations. In addition, methods based on relative proportions of G_1, S and G_2 are robust to possible variations in cell abundances. Here, both approaches corresponded well—rendering growth rates wherein a substantial part of the *Prochlorococcus* HLII population divided twice per day.

Our results highlight a second important ecological result—the large variation in cell abundances, which we propose reflects growth and mortality. We suggest the marked cell losses reflect high mortality, and a link between growth and mortality has been shown for *Prochlorococcus*, albeit at much lower growth rates, for example, Ribalet et al. (2015). Recent work indicates the proportion of *Prochlorococcus*

that are virally infected in the field is low (Mruwat et al., 2021), suggesting that here grazing may be the more prominent force of mortality. This corresponds well with the recent recognition that many protistan predators feed on *Prochlorococcus* (Wilken et al., 2023).

CONCLUSIONS

A limited understanding of major regionally dependent differences in the growth rate of abundant phytoplankton like *Prochlorococcus* may contribute to serious underestimates of its contributions to primary production. This, in turn, impacts both the determination of key taxa in food webs and global carbon cycle estimates. Our findings call for more concerted efforts to determine the growth rates of phytoplankton in the field with attention to the possibility of key differences across biogeochemical provinces.

AUTHOR CONTRIBUTIONS

Jonathan Grone: Writing – original draft; visualization; formal analysis. **Camille Poirier:** Conceptualization; investigation; writing – review and editing; formal analysis. **Kathleen Abbott:** Visualization; formal analysis; writing – review and editing. **Fabian Wittmers:** Formal analysis; visualization; writing – review and editing. **Gualtiero Spiro Jaeger:** Conceptualization; investigation. **Amala Mahadevan:** Conceptualization; investigation. **Alexandra Z. Worden:** Conceptualization; funding acquisition; writing – original draft; methodology; formal analysis; project administration; supervision; resources.

ACKNOWLEDGEMENTS

We thank the captain and crew of the R/V Thomas G. Thompson, Dr. Emily Shroyer, and Worden lab members. Fabian Wittmers was supported by BIOS-SCOPE (Simons Foundation International). Kathleen Abbott was supported by an NSF Graduate Research Fellowship. Funding for this study was provided by ONR grant N000014-17-1-2390 (Amala Mahadevan and Gualtiero Spiro Jaeger) and by the Gordon and Betty Moore Foundation (GBMF 3788) and NSF Dimensions 2230811 to Alexandra Z. Worden as well as the BIOS-SCOPE project (Simons Foundation International). We thank two anonymous reviewers for their constructive criticisms. Open Access funding enabled and organized by Projekt DEAL.

CONFLICT OF INTEREST STATEMENT

The authors declare no conflict of interest.

DATA AVAILABILITY STATEMENT

The data that supports the findings of this study are available in the supplementary material of this article: Datasheet A: Flow cytometric counts for *Prochlorococcus*, *Synechococcus* and picoeukaryotic phytoplankton for samples from CTD casts; Datasheet B: Flow cytometry counts and environmental factors for surface samples of 2015 (Strauss et al., 2023) and 2018 (this study); Datasheet C: Amplicon sequences of *Prochlorococcus* ASVs; Datasheet D: Relative abundances of *Prochlorococcus* ecotypes and HLII oligotypes for surface samples from CTD casts; Datasheet E: Flow cytometry counts and relative abundances of *Prochlorococcus* ecotypes and HLII oligotypes for samples from the diel survey. 16S rRNA gene V1-V2 amplicon data are available through NCBI (BioProject PRJNA935330): https://www.ncbi.nlm.nih.gov/bioproject/PRJNA935330.

ORCID

Alexandra Z. Worden https://orcid.org/0000-0002-9888-9324

REFERENCES

Agawin, N.S.R. & Agustí, S. (2005) *Prochlorococcus* and *Synechococcus* cells in the Central Atlantic Ocean: distribution, growth and mortality grazing rates. *Vie et Milieu*, 55, 165–175.

Ahlgren, A.A., Perelman, J.N., Yeh, Y.-C. & Fuhrman, J.A. (2019) Multi-year dynamics of fine-scale marine cyanobacterial populations are more strongly explained by phage interactions than abiotic, bottom-up factors. *Environmental Microbiology*, 21, 2948–2963.

Angelova, A.G., Ellis, G.A., Wijesekera, H.W. & Vora, G.J. (2019) Microbial composition and variability of natural marine planktonic and biofouling communities from the Bay of Bengal. *Frontiers in Microbiology*, 10, 2738.

Becton Dickinson and Company. (2023) FlowJo™ Software for Mac.

Biller, S.J., Berube, P.M., Lindell, D. & Chisholm, S.W. (2015) *Prochlorococcus*: the structure and function of collective diversity. *Nature Reviews Microbiology*, 13, 13–27.

Callahan, B.J., McMurdie, P.J., Rosen, M.J., Han, A.W., Johnson, A.J.A. & Holmes, S.P. (2016) DADA2: high-resolution sample inference from Illumina amplicon data. *Nature Methods*, 13, 581–583.

Demir-Hilton, E., Sudek, S., Cuvelier, M.L., Gentemann, C.L., Zehr, J.P. & Worden, A.Z. (2011) Global distribution patterns of distinct clades of the photosynthetic picoeukaryote *Ostreococcus*. *The ISME Journal*, 5, 1095–1107.

Eren, A.M., Maignien, L., Sul, W.J., Murphy, L.G., Grim, S.L., Morrison, H.G. et al. (2013) Oligotyping: differentiating between closely related microbial taxa using 16S rRNA gene data. *Methods in Ecology & Evolution*, 4, 1111–1119.

Grob, C., Ulloa, O., Claustre, H., Huot, Y., Alarcón, G. & Marie, D. (2007) Contribution of picoplankton to the total particulate organic carbon concentration in the eastern South Pacific. *Biogeosciences*, 4, 837–852.

Gu, B., Liu, J., Cheung, S., Ho, N.H.E., Tan, Y. & Xia, X. (2022) Insights into prokaryotic community and its potential functions in nitrogen metabolism in the Bay of Bengal, a pronounced oxygen minimum zone. *Microbiology Spectrum*, 10, e0089221.

Hoadley, K.D., Hamilton, M., Poirier, C.L., Choi, C.J., Yung, C.-M. & Worden, A.Z. (2021) Selective uptake of pelagic microbial community members by Caribbean reef corals. *Applied and Environmental Microbiology*, 87, e03175-20.

Landry, M.R., Hood, R.R., Davies, C.H., Selph, K.E., Antoine, D., Carl, M.C. et al. (2022) Microbial community biomass, production and grazing along 110°E in the eastern Indian Ocean. *Deep Sea Research Part II: Topical Studies in Oceanography*, 202, 105134.

Larkin, A.A., Garcia, C.A., Ingoglia, K.A., Garcia, N.S., Baer, S.E., Twining, B.S. et al. (2020) Subtle biogeochemical regimes in the Indian Ocean revealed by spatial and diel frequency of *Prochlorococcus* haplotypes. *Limnology and Oceanography*, 65, 220–232.

Larkin, A.A., Hagstrom, G.I., Brock, M.L., Garcia, N.S. & Martiny, A.C. (2023) Basin-scale biogeography of *Prochlorococcus* and SAR11 ecotype replication. *The ISME Journal*, 17, 185–194.

Liu, H., Landry, M.R., Vaulot, D. & Campbell, L. (1999) *Prochlorococcus* growth rates in the central equatorial Pacific: an application of the f_{max} approach. *Journal of Geophysical Research*, 104, 3391–3399.

Löscher, C.R. (2021) Reviews and syntheses: trends in primary production in the Bay of Bengal—is it at a tipping point? *Biogeosciences*, 18, 4953–4963.

Mahadevan, A., Paluszkiewicz, T., Ravichandran, M., Sengupta, D. & Tandon, A. (2016) Introduction to the special issue on the Bay of Bengal: from monsoons to mixing. *Oceanography*, 29, 14–17.

Martin, M. (2011) Cutadapt removes adapter sequences from high-throughput sequencing reads. *EMBnet Journal*, 17, 10.

McDougall, T.J. & Barker, P.M. (2011) Getting started with TEOS-10 and the Gibbs Seawater (GSW) oceanographic toolbox. *Scor/-lapso WG*, 127, 1–28.

Mitbavkar, S., Anil, A.C., Narale, D.D., Chitari, R., Rao, V.T. & Gopalakrishna, V.V. (2020) Environmental influence on the picophytoplankton community structure in the central and northern Bay of Bengal. *Regional Studies in Marine Science*, 40, 101528.

Mruwat, N., Carlson, M.C.G., Goldin, S., Ribalet, F., Kirzner, S., Hulata, Y. et al. (2021) A single-cell polony method reveals low levels of infected *Prochlorococcus* in oligotrophic waters despite high cyanophage abundances. *The ISME Journal*, 15, 41–54.

R Core Team. (2023) R: A language and environment for statistical computing.

Reckermann, M. & Veldhuis, M.J. (1997) Trophic interactions between picophytoplankton and micro- and nanozooplankton in the western Arabian Sea during the NE monsoon 1993. *Aquatic Microbial Ecology*, 12, 263–273.

Ribalet, F., Swalwell, J., Clayton, S., Jiménez, V., Sudek, S., Lin, Y. et al. (2015) Light-driven synchrony of *Prochlorococcus* growth and mortality in the subtropical Pacific gyre. *Proceedings of the National Academy of Sciences of the United States of America*, 112, 8008–8012.

RStudio Team. (2022) RStudio: integrated development for R.

Shalapyonok, A., Olson, R.J. & Shalapyonok, L.S. (1998) Ultradian growth in *Prochlorococcus* spp. *Applied and Environmental Microbiology*, 64, 1066–1069.

Spiro Jaeger, G., Mackinnon, J.A., Lucas, A.J., Shroyer, E., Nash, J., Tandon, A. et al. (2020) How spice is stirred in the Bay of Bengal. *Journal of Physical Oceanography*, 50, 2669–2688.

Strauss, J., Choi, C.J., Grone, J., Wittmers, F., Jimenez, V., Makareviciute-Fichtner, K. et al. (2023) The Bay of Bengal exposes abundant photosynthetic picoplankton and newfound diversity along salinity-driven gradients. *Environmental Microbiology*, 25, 2118–2141.

Sudek, S., Everroad, R.C., Gehman, A.-L.M., Smith, J.M., Poirier, C.L., Chavez, F.P. et al. (2015) Cyanobacterial distributions along a physico-chemical gradient in the Northeastern Pacific Ocean. *Environmental Microbiology*, 17, 3692–3707.

Thompson, A.W., Kouba, K. & Ahlgren, N.A. (2021) Niche partitioning of low-light adapted *Prochlorococcus* subecotypes across oceanographic gradients of the North Pacific Subtropical Front. *Limnology and Oceanography*, 66, 1548–1562.

van Rossum, G. & Drake, F.L. (1995) Python reference manual.

Vaulot, D., Marie, D., Olson, R.J. & Chisholm, S.W. (1995) Growth of *Prochlorococcus*, a photosynthetic prokaryote, in the Equatorial Pacific Ocean. *Science*, 268, 1480–1482.

Vergin, K.L., Beszteri, B., Monier, A., Cameron Thrash, J., Temperton, B., Treusch, A.H. et al. (2013) High-resolution SAR11 ecotype dynamics at the Bermuda Atlantic Time-series Study site by phylogenetic placement of pyrosequences. *The ISME Journal*, 7, 1322–1332.

Wei, Y., Huang, D., Zhang, G., Zhao, Y. & Sun, J. (2020) Biogeographic variations of picophytoplankton in three contrasting seas: The Bay of Bengal, South China Sea and western Pacific Ocean. *Aquatic Microbial Ecology*, 84, 91–103.

Wilken, S., Yung, C.C.M., Poirier, C., Massana, R., Jimenez, V. & Worden, A.Z. (2023) Choanoflagellates alongside diverse uncultured predatory protists consume the abundant open-ocean cyanobacterium *Prochlorococcus*. *Proceedings of the National Academy of Sciences of the United States of America*, 120, e2302388120.

Worden, A.Z., Nolan, J.K. & Palenik, B. (2004) Assessing the dynamics and ecology of marine picophytoplankton: the importance of the eukaryotic component. *Limnology and Oceanography*, 49, 168–179.

SUPPORTING INFORMATION

Additional supporting information can be found online in the Supporting Information section at the end of this article.

How to cite this article: Grone, J., Poirier, C., Abbott, K., Wittmers, F., Jaeger, G.S., Mahadevan, A. et al. (2024) A single *Prochlorococcus* ecotype dominates the tropical Bay of Bengal with ultradian growth. *Environmental Microbiology*, 26(3), e16605. Available from: https://doi.org/10.1111/1462-2920.16605